



## Article

# Stress Characteristic Analysis of Pump-Turbine Head Cover Bolts during Load Rejection Based on Measurement and Simulation

Xingxing Huang <sup>1</sup> , Liu Chen <sup>2</sup>, Zhengwei Wang <sup>3,\*</sup> , Haibo Li <sup>4</sup>, Shunyi Chen <sup>5</sup>, Kun Hu <sup>4</sup>, Chengjun Li <sup>5</sup> and Lan Qiu <sup>4</sup>

<sup>1</sup> S.C.I. Energy, Future Energy Research Institute, Seidengasse 17, 8706 Zurich, Switzerland

<sup>2</sup> China Institute of Water Resources and Hydropower Research, No. 20, Chegongzhuang West Road, Beijing 100048, China

<sup>3</sup> State Key Laboratory of Hydrosience and Engineering, Department of Energy and Power Engineering, Tsinghua University, Beijing 100084, China

<sup>4</sup> Huadong Yixing Pumped Storage Co., Ltd., No. 3 Qinhu Road, Yixing City 214256, China

<sup>5</sup> Powerchina Huadong Engineering Corporation Limited, No. 201 Gaoxiao Road, Hangzhou 311122, China

\* Correspondence: wzw@mail.tsinghua.edu.cn

**Abstract:** It is not uncommon for pump-turbine units in pumped storage power plants to experience load rejections due to the sudden disconnection of the generator from the power grid. Load rejection can suddenly increase the rotating speed of the pump-turbine and cause strong pressure fluctuations in the flow passage of the pump-turbine unit. During load rejection, the strong pressure fluctuations caused by the water hammer effect can cause strong structural vibrations, high stresses and even damage to the turbine runner, head cover, stay ring, bottom ring, head cover bolts and bottom ring bolts. In order to study, in detail, the flow-induced stress characteristics of the prototype pump-turbine unit, and the pressure variations during load rejection in a high-head pumped storage power plant were measured first. Then the measured data were used to set up computational fluid dynamics (CFD) simulations in the entire flow passage of the prototype pump-turbine and to calibrate the simulation results. The calculated pressure distributions in the flow passage during load rejection were exported and mapped on the finite element model of the stationary structures of the pump-turbine unit so that the flow-induced stresses on the head cover, stay ring, bottom ring, head cover bolts and bottom ring bolts can be calculated. The results of the analysis show that the maximum stresses in the head cover bolts and bottom ring bolts are located on the rounded corner of the bolt near the stay ring and that the stresses in the bolts vary with time during load rejection. The maximum stresses of the head cover bolts are higher than the maximum stresses of the bottom ring bolts, and the maximum stresses of the bolts are above two-thirds of the yield strength of the bolt material. It is recommended to use larger nominal diameter bolts to avoid damage to the connecting bolts of the pump-turbine unit.

**Keywords:** prototype pump-turbine; load rejection; head cover bolts; flow-induced stress analysis; measurement and simulation



**Citation:** Huang, X.; Chen, L.; Wang, Z.; Li, H.; Chen, S.; Hu, K.; Li, C.; Qiu, L. Stress Characteristic Analysis of Pump-Turbine Head Cover Bolts during Load Rejection Based on Measurement and Simulation. *Energies* **2022**, *15*, 9496. <https://doi.org/10.3390/en15249496>

Academic Editor: Tong Seop Kim

Received: 26 October 2022

Accepted: 12 December 2022

Published: 14 December 2022

**Publisher's Note:** MDPI stays neutral with regard to jurisdictional claims in published maps and institutional affiliations.



**Copyright:** © 2022 by the authors. Licensee MDPI, Basel, Switzerland. This article is an open access article distributed under the terms and conditions of the Creative Commons Attribution (CC BY) license (<https://creativecommons.org/licenses/by/4.0/>).

## 1. Introduction

Pumped storage power stations (PSPSs) have been built in various countries to increase the flexibility of the power grid and improve its power quality. Due to the power regulation of the grid, pump-turbine (PT) units must often actively or passively undergo load rejection during power generation. When the PT unit suddenly loses the grid load, the huge energy generated by the water flow makes the unit speed rise rapidly, and the PT unit governor quickly closes the guide vanes, and after a few moments, the PT unit will be stabilized again in the speed no-load condition. After a short period of time, the PT unit will stabilize again at speed no-load or stop. During load rejection of a high-head PSPS, the water hammer

effect caused by the rapid closure of the guide vanes can lead to strong pressure pulsations in the flow channel of the PT unit and result in strong vibrations on the structures of the unit, including turbine runner, head cover, stay ring, bottom ring, head cover bolts, bottom ring bolts, etc.

It is not uncommon to see reports on the serious accidents and structural damage of the hydroelectric units in hydropower plants, including PSPSs caused by poor design, unreasonable operation and drastic pressure fluctuations during transient processes, including load rejection [1–5]. Many researchers have investigated the unsteady flow characteristics of various prototype hydraulic turbine units during load rejection [6–10]. Studies [10–14] have compared the flow results of computational fluid dynamics (CFD) calculations of hydraulic turbine units, including PT units, with the results of the field measurements and have verified the accuracy of numerical simulations. Studies [15–18] have proposed a CFD method to calculate the fluid flow at various critical time points during transient processes and studied the main stress changes of the PT structures caused by the high pressure of the transient flow.

Plenty of investigations [13,19–25] have studied the structural stresses of the PT units under stable operating conditions and during transient processes and also validated the accuracy of the flow-induced stress calculation method, and some investigations [26–32] have analyzed the stresses of the head cover bolts of different PT units during transient processes, such as start-up and shut-down in turbine mode and pump mode. However, only a very limited number of studies [33] have focused on the analysis of the flow-induced stress characteristics of the head cover bolts and bottom ring bolts during load rejection in PT units. Since the stationary structure of the PT unit, consisting of the head cover, stay ring, bottom ring, head cover bolts and bottom ring bolts, is subjected to high stresses caused by high levels of pulsating pressure during load rejection, which is one of the challenging processes for PT units.

The bolt load under the load rejection is significantly larger than that under the rated operation condition and is more complicated. Specifically, the maximum stress of the head cover bolts under the rated operating condition of the investigated PT unit has exceeded 2/3 of the yield strength of the bolt material. Therefore, in order to ensure the operational safety of the PT unit, it is of great significance to analyze the unsteady flow-induced stress characteristics of the head cover bolts during load rejection in detail and judge the safety of the bolts. In this investigation, the prototype PT unit in a high-head PSPS was first measured on-site during the load rejection process. Then, 3D unsteady CFD simulations of the flow passage during load rejection were performed using the measured data of inlet and outlet pressures, rotating speeds and guide vane openings. Next, the pressure files in the flow passage during load rejection were exported from the CFD analysis and applied sequentially to the finite element model of the stationary structure of the PT unit via the one-way fluid-structure coupling method. Finally, the characteristics of flow-induced stresses in the head cover, stay ring, bottom ring, head cover bolts and bottom ring bolts were analyzed and discussed in detail. Based on the conclusions drawn from this study, useful recommendations are given that are feasible in hydropower engineering practice to avoid bolt fractures in PT units.

## 2. Field Measurement

The investigated PT unit is installed in a high-head PSPS with a rated head of 363 m and rated power of 255 MW (Figure 1). The PT has 9 blades with a diameter of 4.4 m, and the inlet height is around 1% of D1. The main geometrical parameters and design parameters of the investigated PT unit are listed in Table 1.

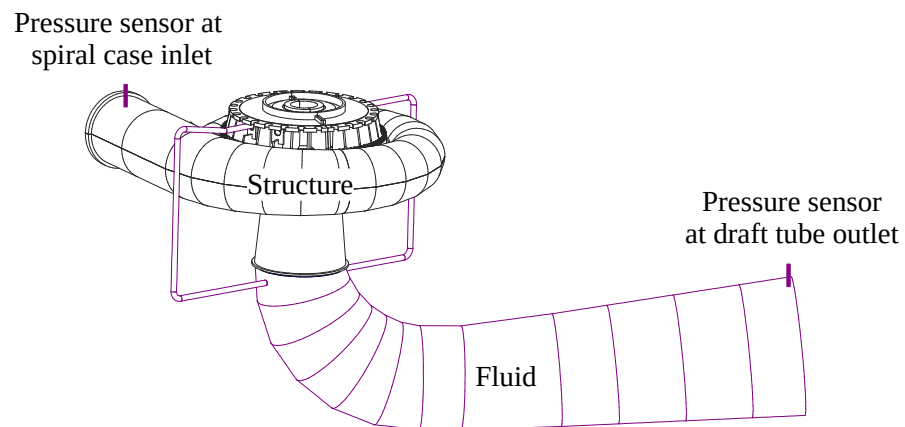


**Figure 1.** The structural and fluid model of the investigated pump turbine.

**Table 1.** Basic parameters of the pump-turbine unit.

Property	Unit	Value
Rated power $P_r$	MW	255
Rated head $H_r$	m	363
Rated rotating speed $n_r$	rpm	375
Runner diameter $D$	m	4.4
Number of stay vanes $N_{sv}$	-	26
Number of guide vanes $N_{gv}$	-	26
Number of runner blades $N_b$	-	9

During the construction of the PSPS, pressure sensors were installed in the PT units as part of an online monitoring and fault diagnosis system to ensure the long-term safe operation of the unit. Figures 1 and 2 show the locations of pressure sensors, which were installed in the spiral case inlet, draft tube outlet, the vaneless space between the guide vanes and runner blades and the crown chamber and the band chamber, respectively. The accuracy of the pressure sensor is  $\pm 0.25\%$ FS. The measured pressure, rotating speed and other non-electrical signals were converted into 4–20 mA electrical signals by the sensors and sent to the power plant computer supervisory system for monitoring and control of the unit.

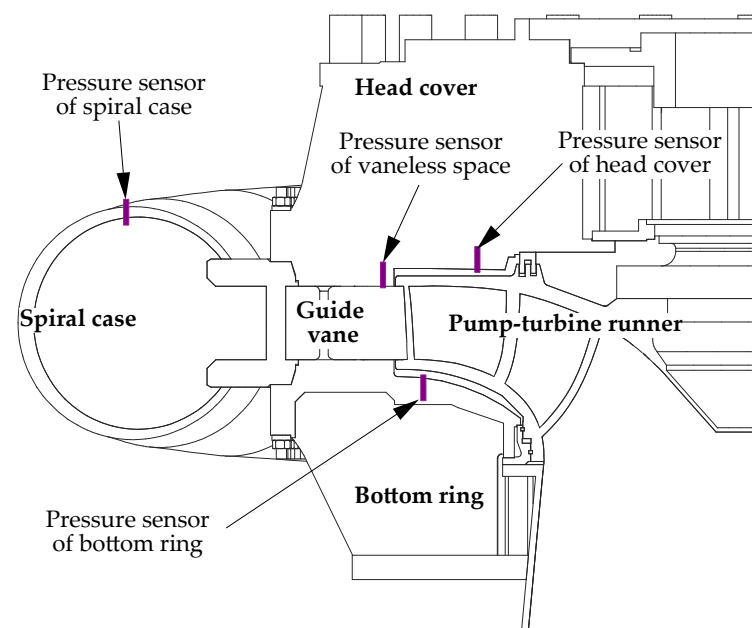


**Figure 2.** Locations of the installed pressure sensors of the PT unit (sectional view).

The on-site measurement was conducted during the process of the load rejection of the PT unit. As shown in Figure 3, the operating parameters, such as the rotating speed, the pressure at the spiral case inlet, the pressure at the draft tube outlet, the pressure at the vaneless space, the pressure at the crown chamber and the pressure at the band chamber, changed drastically during the transient process of the load rejection. The pressure values of each pressure sensor in Figure 3 were normalized with reference to the maximum pressure at the spiral case inlet during load rejection, and the rotating speed was normalized with reference to the rated rotating speed.

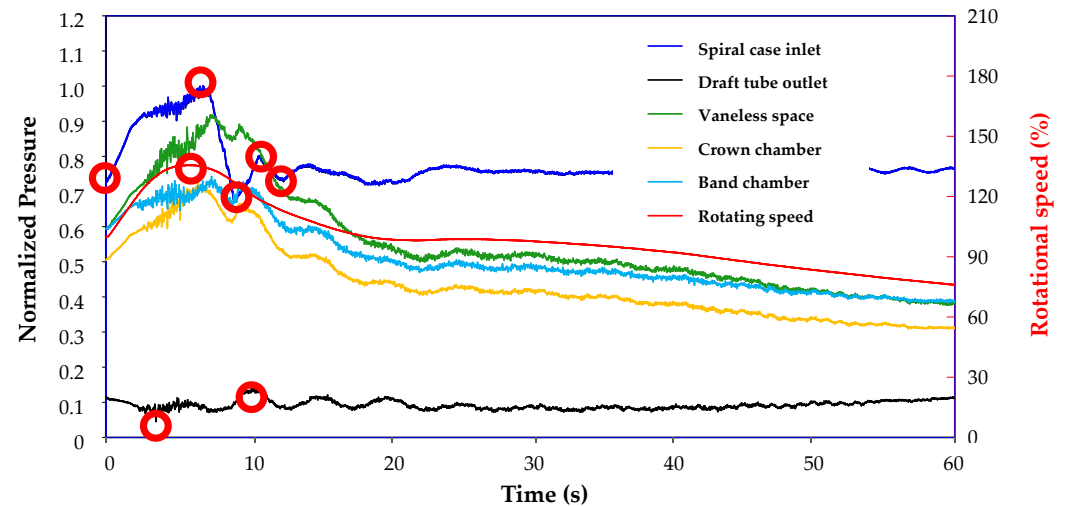


Figure 3. The measured parameters of the pump-turbine unit during load rejection.

As marked with red circles in Figure 3, eight moments at the extreme values of the measured data in the first 12 s during the load rejection of the PT unit were selected for 3D flow simulations (Table 2). After 12 s in the load rejection process, the PT unit slowed down, and the flow changes were not as drastic as before. The measured pressure values of the spiral case inlet and the draft tube outlet, rotating speed and guide vane opening at different moments were used to set up the boundary conditions and initial conditions of the CFD analysis.

Table 2. Parameters of boundary conditions and initial conditions of the CFD analysis.

Time (s)	Description	Pressure at Spiral Case Inlet (%)	Pressure at Draft Tube Outlet (%)	Rotating Speed (%)	Guide Vane Opening (%)
0.0	Rated load	73.0	11.5	100.0	100.0
3.4	Minimum pressure at draft tube outlet	93.4	4.5	130.1	64.7
5.7	Maximum rotating speed	97.4	10.2	135.6	49.9
6.6	Maximum pressure at spiral case inlet	100.0	9.1	134.8	45.0
8.7	Minimum pressure at spiral case inlet	67.7	9.8	127.1	35.7
9.8	Maximum pressure at draft tube outlet	75.0	13.9	120.9	33.2
10.3	Local maximum pressure at spiral case inlet	80.1	13.1	118.7	31.7
12.0	Local minimum pressure at spiral case inlet	73.2	8.6	112.7	25.8

### 3. Methods of Numerical Simulation

#### 3.1. Governing Equations of 3D Fluid Dynamics Analysis

In this study, the Reynolds-averaged Navier–Stokes (RANS) equations are used to perform the 3D fluid dynamics analysis, and the water in the pump-turbine unit is treated as a viscous incompressible Newtonian fluid. The mass and momentum conservation equations for the flow are described below using Einstein's summation convention in Cartesian coordinates.

$$\frac{\partial \bar{u}_i}{\partial x_i} = 0 \quad (1)$$

$$\frac{\partial \bar{u}_i}{\partial t} + \frac{\partial \bar{u}_i \bar{u}_j}{\partial x_j} = -\frac{1}{\rho} \frac{\partial \bar{p}}{\partial x_i} + \frac{\partial}{\partial x_j} \left[ \nu \left( \frac{\partial \bar{u}_i}{\partial x_j} + \frac{\partial \bar{u}_j}{\partial x_i} \right) \right] - \frac{\partial \overline{u'_i u'_j}}{\partial x_j} + \bar{f}_i \quad (2)$$

where  $x_i$  and  $x_j$  are the Cartesian coordinate directions,  $\bar{u}_i$  and  $\overline{u'_i}$  are the time-averaged term and fluctuating term of the fluid velocity,  $t$  is time,  $\rho$  is the density of the water,  $\bar{p}$  is the time-averaged pressure,  $\overline{u'_i u'_j}$  is the Reynolds stress term and  $\bar{f}_i$  represents time-averaged external forces.

The  $k - \omega$  shear stress transport (SST) turbulence model is used to simulate the unstable, turbulent flow in the pump-turbine flow channels. The  $k - \omega$  SST model integrates the advantages of the  $k - \omega$  model and the  $k - \epsilon$  model and can accurately predict flow separation and near-wall flow [34].

#### 3.2. Governing Equations of the 3D Flow-Induced Stress Analysis

The finite element method (FEM) is widely used to calculate the structural stresses of pump-turbine units. The governing equation of flow-induced structural dynamics can be described as

$$[M]\{\ddot{d}\} + [C]\{\dot{d}\} + [K]\{d\} = \{F(t)\} + \{F_f(t)\} \quad (3)$$

where  $[M]$ ,  $[C]$  and  $[K]$  are the mass matrix, damping matrix and stiffness matrix of the structure, respectively;  $\{d\}$ ,  $\{\dot{d}\}$  and  $\{\ddot{d}\}$  are the vectors of node displacement, velocity and acceleration, respectively;  $\{F(t)\}$  is the external excitation load vector acting on structures,  $\{F_f(t)\}$  represents the fluid pressure load vector acting on the structure.

Applying the pressure distributions calculated by 3D CFD simulation to the structures of the pump-turbine unit, the flow-induced stresses in the structures, including head cover bolts, during the process of load rejection can be analyzed in detail.

$$\{\sigma\} = [E][S_d]\{u\} \quad (4)$$

where  $[E]$  is the elasticity matrix of the structure, and  $[S_d]$  represents the strain-displacement matrix of the structure.

The equivalent stress  $\sigma_{vM}$  (Equation (5)) is used to evaluate the stress characteristics of structures of the pump-turbine unit during load rejection.

$$\sigma_{Eqv} = \sqrt{0.5[(\sigma_I - \sigma_{II})^2 + (\sigma_{II} - \sigma_{III})^2 + (\sigma_{III} - \sigma_I)^2]} \quad (5)$$

where  $\sigma_I$ ,  $\sigma_{II}$ ,  $\sigma_{III}$  are the maximum, middle and minimum principal stresses, respectively.

### 4. Numerical Simulation of the Fluid Flow

#### 4.1. Three-Dimensional Flow Simulation Model

The 3D model of the pump-turbine unit is shown in Figure 4, including spiral case passage, stay vane passage, guide vane passage, runner passage, draft tube passage, crown chamber, band chamber, upper and lower labyrinth seals and pressure balance pipes.

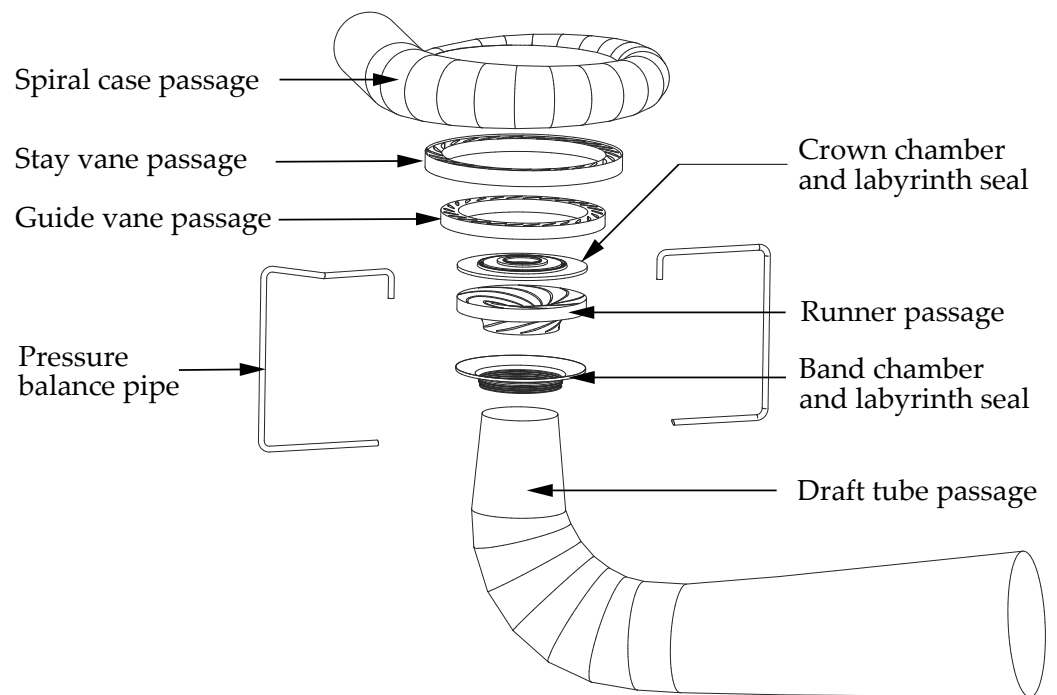


**Figure 4.** The 3D modeling of the flow passage of the pump-turbine unit.

In this work, ANSYS CFX5 solver was used to carry out the 3D CFD simulations. The analysis type and solver type were set to stable and high-resolution, respectively. The turbulence model was set to  $k - \omega$  SST and the turbulence mathematical accuracy was set to first-order with a convergence residual of  $10^{-5}$ . The pressure values at the spiral case inlet and at the draft tube outlet were directly taken from the measurements shown in Figure 3. The runner passage was defined as a rotational domain, and the rotating speed over time during load rejection was specified based on the measured values. The other fluid passages were defined as stationary domains. The interfaces between guide vanes and runner and runner and draft tube were set to Frozen Rotor, and the others are set to general connection. A non-slip wall was used as the wall boundary conditions.

Hybrid meshes with tetrahedral and hexahedral elements were used to mesh fluid passages. According to the guide vane opening angles during the load rejection, the meshes of the guide vane channels were also updated. To achieve a more precise result at the boundary layer of the flow passages, the meshes near the wall boundaries of all fluid domains were refined. The average  $Y_{plus}$  value of the mesh was in the range of 30 to 100 for the flow passage.

Three groups of finite volume meshes, consisting of 6.96 million, 9.46 million and 10.2 million elements, were created to perform the mesh sensitivity analysis. The simulated efficiencies between the inlet of the spiral case and the outlet of the draft tube at the rated load condition within various element amounts were compared with the measured efficiency ( $\eta_{Meas.}$ ) (Figure 5). In order to ensure the accuracy of the simulation results and save computational time, the second group of meshes with 9.46 million elements, marked by the blue box in Figure 5, was utilized to carry out the CFD simulations of the PT unit during the load rejection process.

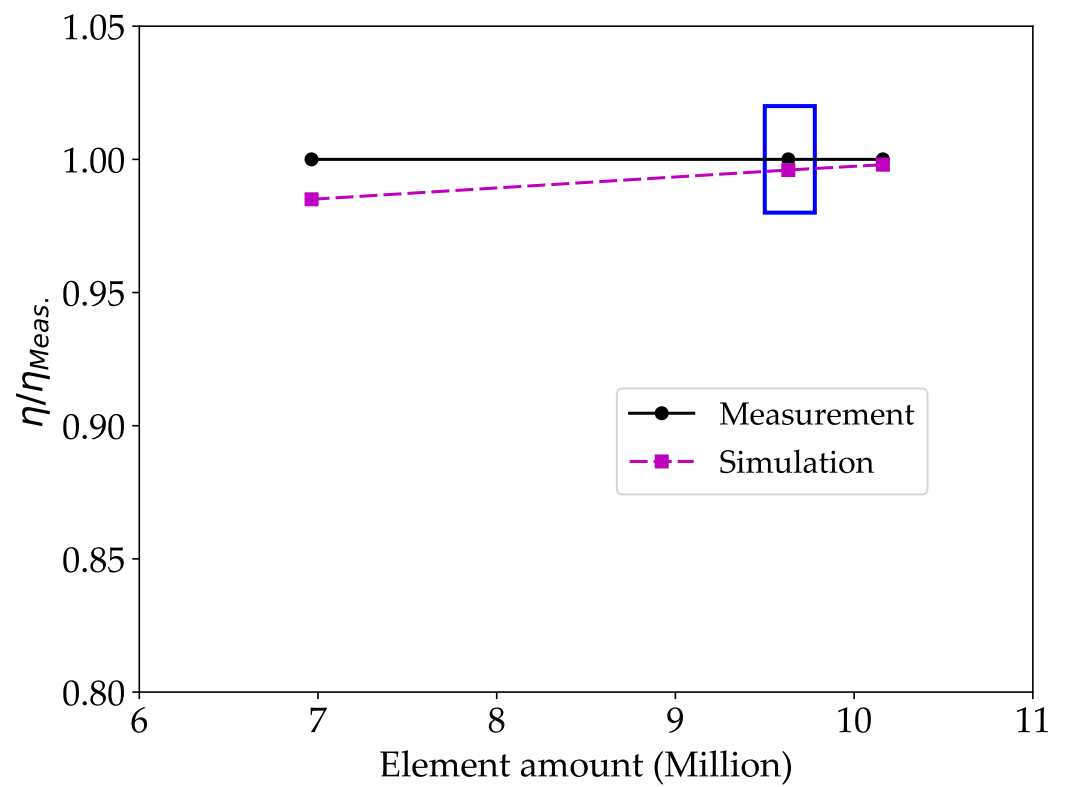


Figure 5. Mesh sensitivity analysis of the CFD simulation.

Figure 6 presents the finite volume mesh of the fluid domains of the investigated pump-turbine unit. And the element amounts of different PT flow passages are listed in Table 3.

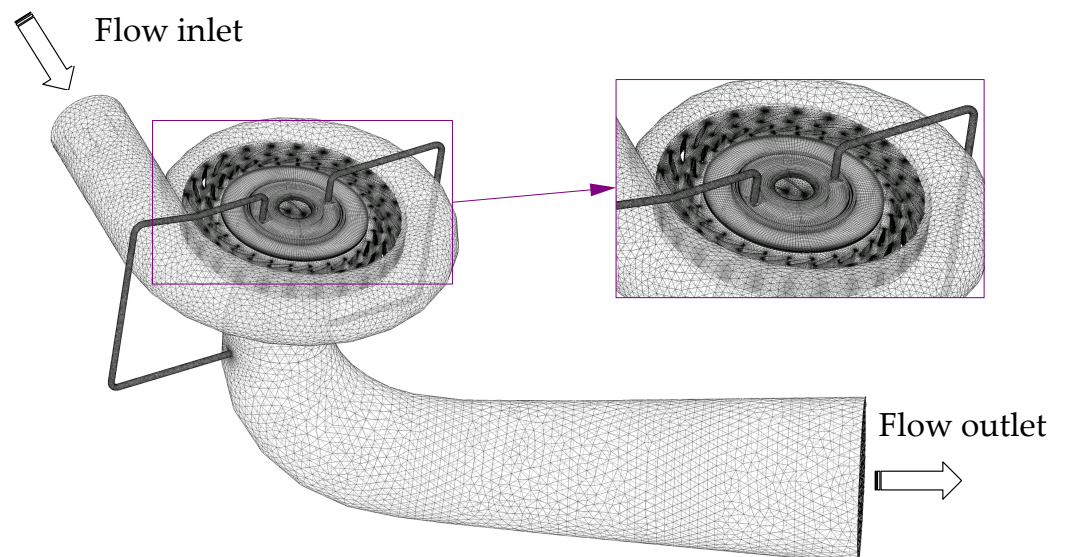


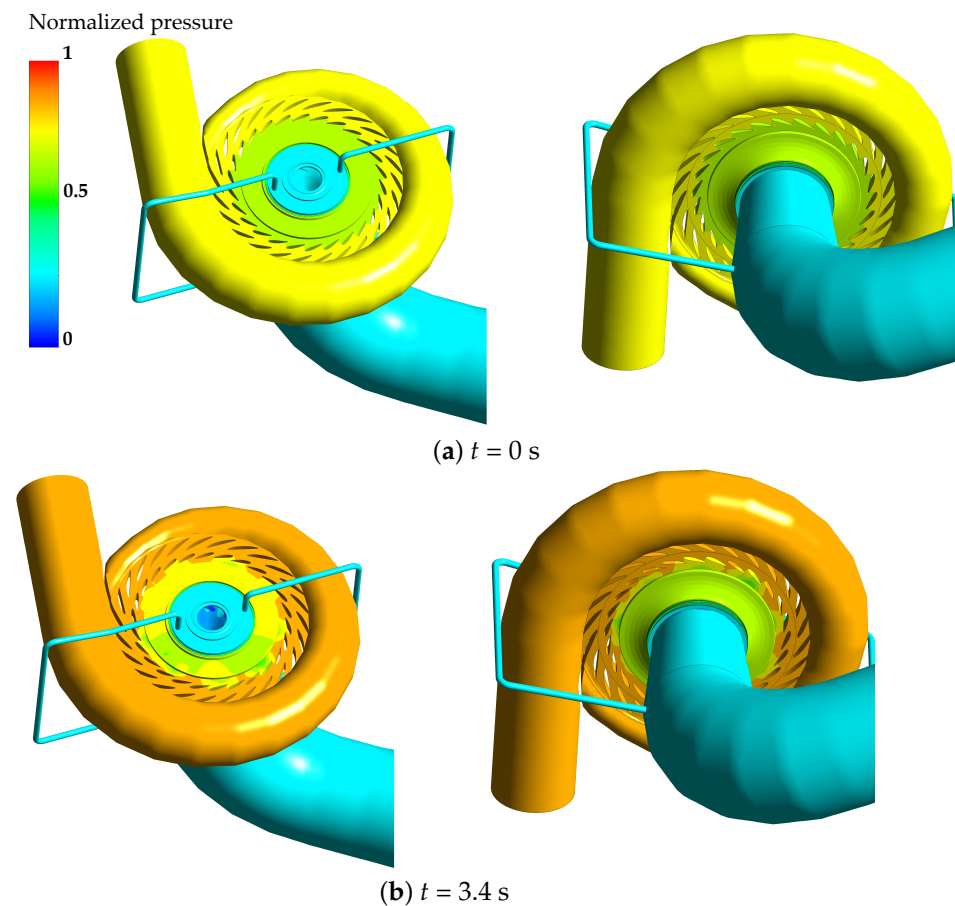
Figure 6. The finite volume mesh of the fluid domains for 3D CFD analysis.

**Table 3.** Element amount of different PT flow passages.

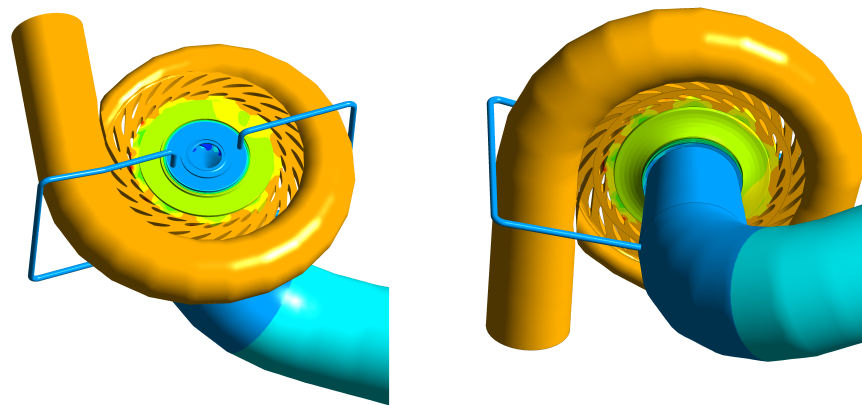
Flow Passage	Element Amount (Million)	Element Type
Spiral case passage	0.11	Tetrahedral and hexahedral
Stay vane passage	3.22	Tetrahedral and hexahedral
Guide Vane passage	0.30	Hexahedral
Crown chamber and labyrinth seal	0.15	Hexahedral
Runner passage	5.23	Tetrahedral and hexahedral
Band chamber and labyrinth seal	0.07	Hexahedral
Draft tube passage	0.17	Tetrahedral and hexahedral
Pressure balance pipes	0.39	Tetrahedral
Total	9.64	Tetrahedral and hexahedral

#### 4.2. Results and Discussions

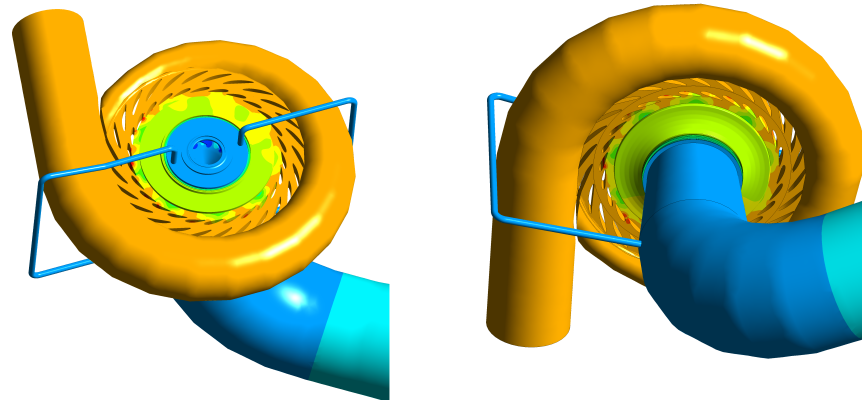
In the load rejection process, the flow of the fluid passages shows extremely unstable turbulent characteristics (Figure 7). At the starting moment ( $t = 0$  s), when the unit works under the full load, the pressure distribution of the unit is relatively stable. From  $t = 3.4$  s, the guide vanes start to close, and the pressure in the spiral case passage is increased due to the water hammer effect. The pressure in the draft tube is also affected by the water hammer effect. The pressure distribution of the crown chamber and band chamber becomes nonuniform, which affects the vibration of the head cover and bottom ring significantly.

**Figure 7.** Cont.

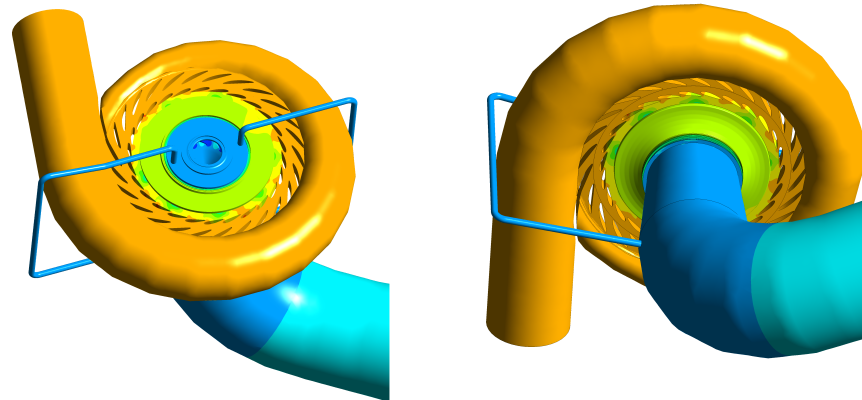




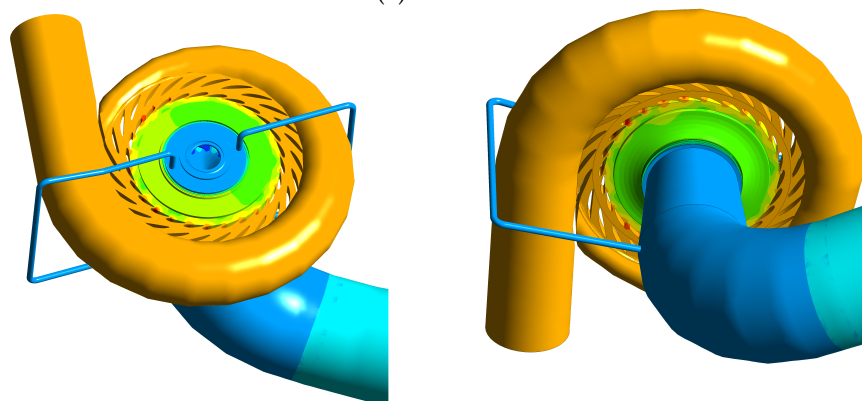
(c)  $t = 5.7$  s



(d)  $t = 6.6$  s

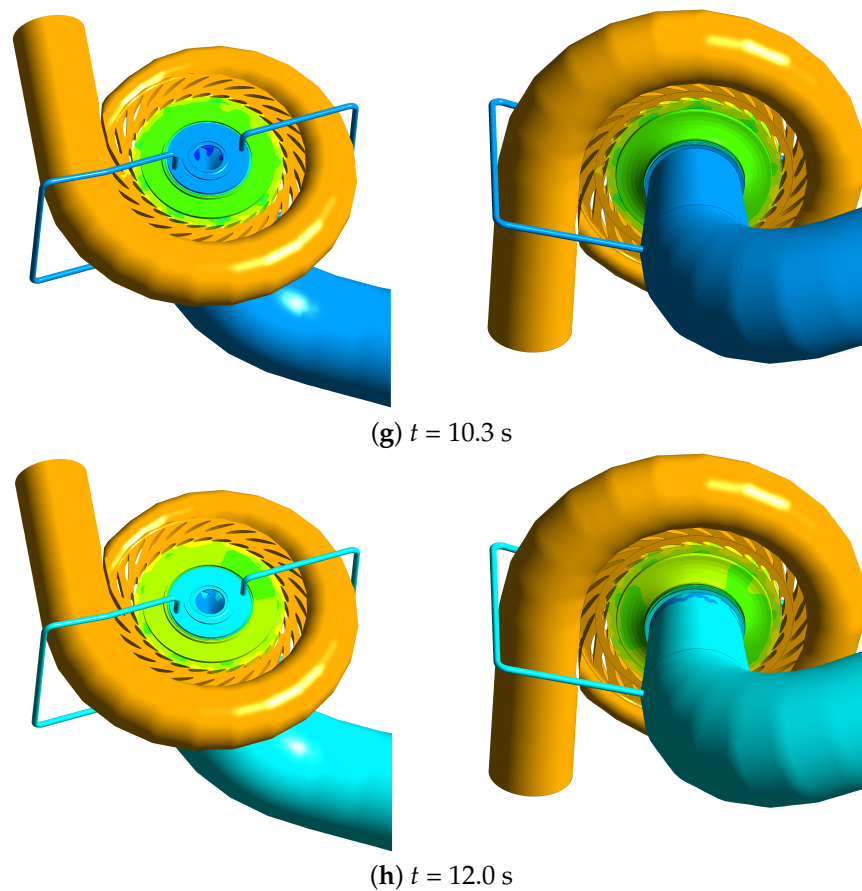


(e)  $t = 8.7$  s



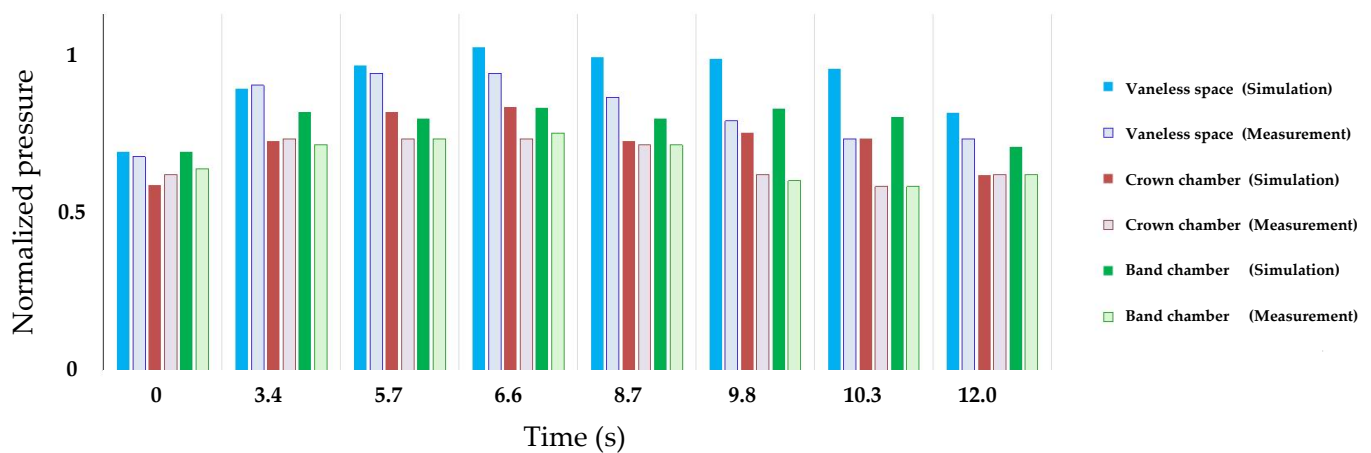
(f)  $t = 9.8$  s

Figure 7. Cont.



**Figure 7.** Pressure distribution in the flow passages at different key time moments.

According to the pressure sensor installation locations shown in Figure 2, the corresponding pressure monitoring points were added to the CFD simulation model to record the pressure values during load rejection at the pressure sensor locations in the vaneless space, crown chamber and band chamber. Figure 8 presents the comparison of the measured and simulated results of the pressure monitoring points at eight calculation times during the load rejection process. It can be seen that the simulation results are in general agreement with the corresponding measurement results.



**Figure 8.** Comparison of the measured and simulated pressure results during load rejection.

Most of the deviations between the simulation and measurement are in the range of 0.3–13%, and the largest deviation is around 27%. The following factors can introduce

deviations between the measurement and the corresponding calculation results. On the one hand, during the load rejection process, the measured parameters, such as rotating speed, guide vane angle and pressure values at the spiral case inlet and at the draft tube outlet, changed rapidly with time. The signal delay of the signal acquisition system during the field measurement may lead to a minor difference in the boundary conditions used in the numerical calculation from the actual ones, resulting in deviations in the results between the simulation and measurement. On the other hand, an ideal model of the PT unit was created from the design drawings for CFD simulations. However, the final geometric model of the PT unit may have small deviations from the ideal model during fabrication at the manufacturing plant and installation at the power plant, which can lead to deviations in the simulation results.

## 5. Flow-Induced Structural Stress Analysis

### 5.1. Simulation Setup

The stationary structures of the investigated pump-turbine unit have a head cover, a stay ring, a bottom ring and connecting bolts (Figure 9). There are a total of 116 head cover bolts and 116 bottom ring bolts. The nominal diameter of these connection bolts is 64 mm (M64). The material properties of the stationary structures are listed in Table 4.

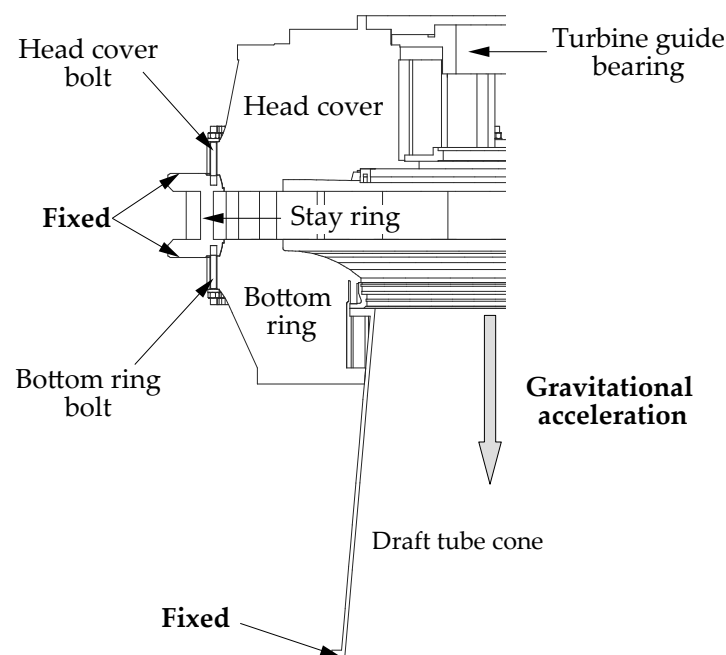


Figure 9. The CAD model of the investigated structures.

Table 4. Material properties of the structures.

Property	Unit	Value
Density	( $\text{g}\cdot\text{m}^{-3}$ )	7850
Modulus of elasticity	(Pa)	$2.1 \times 10^{11}$
Poisson's ratio	(-)	0.3

ANSYS Mechanical is used to perform the structural dynamic behavior analysis. By applying the calculated pressure loads on the stationary structures of the pump-turbine unit, the flow-induced dynamic behavior of the structures, including the head cover bolts and bottom ring bolts, is analyzed in detail.

The surfaces of the stay ring connecting with the concretes are fixed, and the bottom ring surface welded into the draft tube is also fixed (Figure 9). The stiffness of the turbine

guide bearing is  $1 \times 10^9 \text{ N}\cdot\text{m}^{-1}$ ), and the gravity ( $g = 9.8 \text{ m}\cdot\text{s}^{-2}$ ) is taken into consideration for the analysis.

The finite element mesh and the boundary conditions are shown in Figure 10. The geometrically complex head cover, stay ring and bottom ring are meshed with high-quality tetrahedral elements, while the bolts are geometrically simple and meshed with high-quality hexahedral elements. The meshes of the connection bolts are refined to obtain more accurate stress results. In this study, the bolt thread details are not considered.

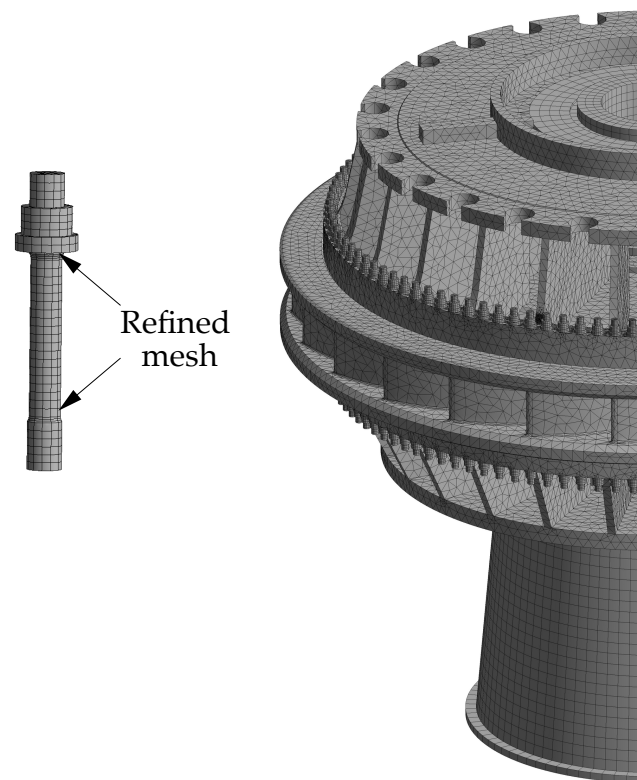


**Figure 10.** Finite element mesh of the stationary structures and the refined mesh of the bolts.

As with the fluid simulation, three sets of finite element meshes containing 1.2 million, 1.6 million and 2.7 million elements were built to perform the mesh sensitivity analysis. The mesh with 1.6 million elements had a similar result to that of the 2.7 million elements but used much less computing time, so it was taken to conduct the following finite element analysis.

The head cover, the stay ring and the bottom ring are assembled into a single structure by applying pretension force to each head cover bolt and bottom ring bolt (Figure 10). As shown in Figure 11, the bolt threads are bonded to the stay ring, and the bolt thread details are not considered in this investigation. The nuts are bonded to the bolt heads. Frictional contact with a friction coefficient of 0.1 is assigned to the connection surfaces between the head cover and the stay ring, the surfaces between the bottom ring and the stay ring and the surfaces between the nuts and the head cover, as well as the surfaces between the nuts and the bottom ring.

The pressure loads calculated by the 3D CFD simulations at each time point during the load rejection are sequentially exported and applied to the finite element model of the stationary structures of the PT unit. Thus the flow-induced stress characteristics of the stationary structures and bolts can be calculated.

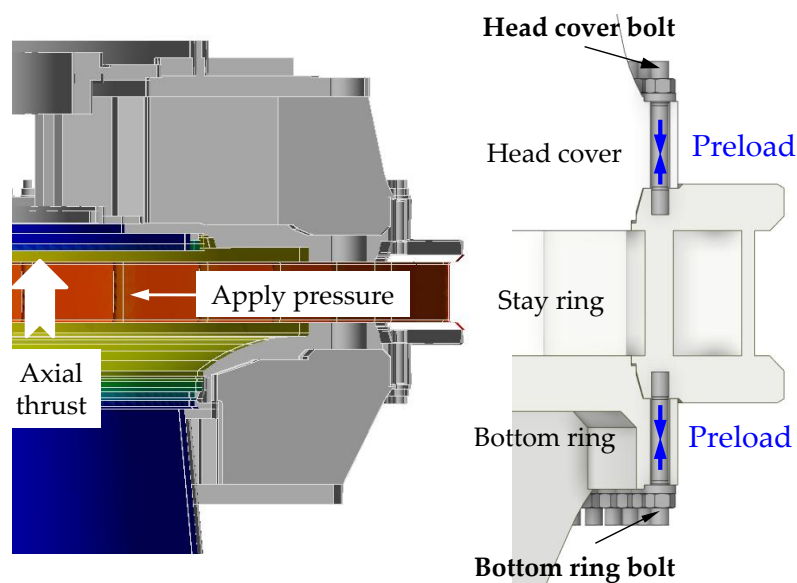


**Figure 11.** The applied loads and boundary conditions of the stationary structures of the PT unit.

### 5.2. Results and Discussion

The stress of the structures induced by unsteady flow during load rejection is changing with time, but the stress distribution at the different moments keeps the same pattern as shown in Figure 12.

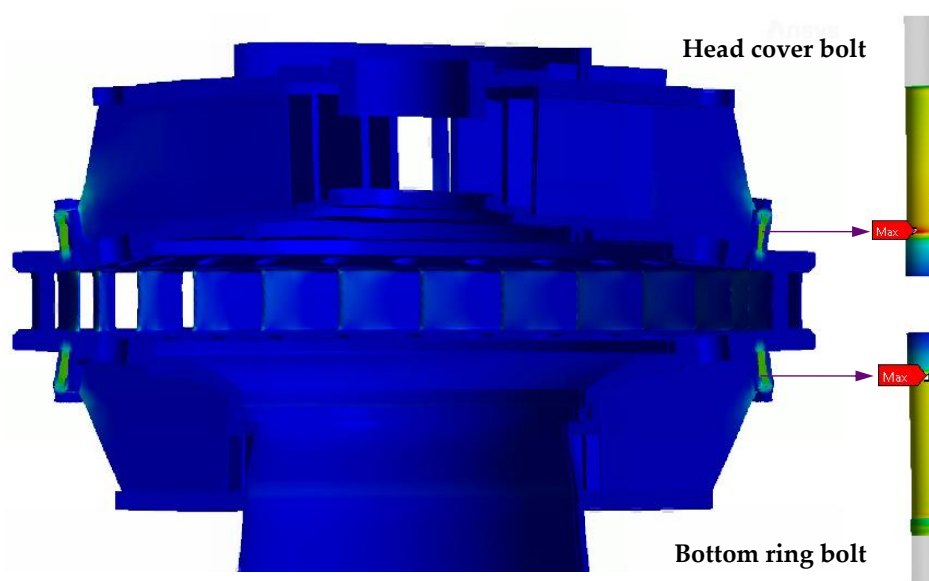


**Figure 12.** The stress distribution of the structure unit during load rejection.

The fluctuating pressures applied to the head cover, and bottom ring lift the head cover up and push the bottom ring down, so the stay vanes will be stretched. The head cover bolts and bottom ring bolts are also heavily stretched, so they are the most damage-prone components of the PT unit. From Figure 12, it can be seen that the maximum stress concentration of the head cover bolts and bottom ring bolts is located at the fillet of the bolt close to the stay ring.

In order to provide more general results as a reference for similar cells, the maximum stresses of the head cover bolts and bottom ring bolts during load rejection were normalized relative to the yield strength of the bolt material (Figure 13). It can be seen that the maximum stress of the bolts during the load rejection process varies with time, and the maximum

stress of the head cover bolts is higher than the bottoming bolts. The ratio of the maximum stress of the bolt to its yield strength during the dumping process is in the range of 0.82–0.94, which is much larger than  $2/3$  of the yield strength limit. Therefore, the head cover bolts and bottom ring bolts are indeed in a very dangerous condition.

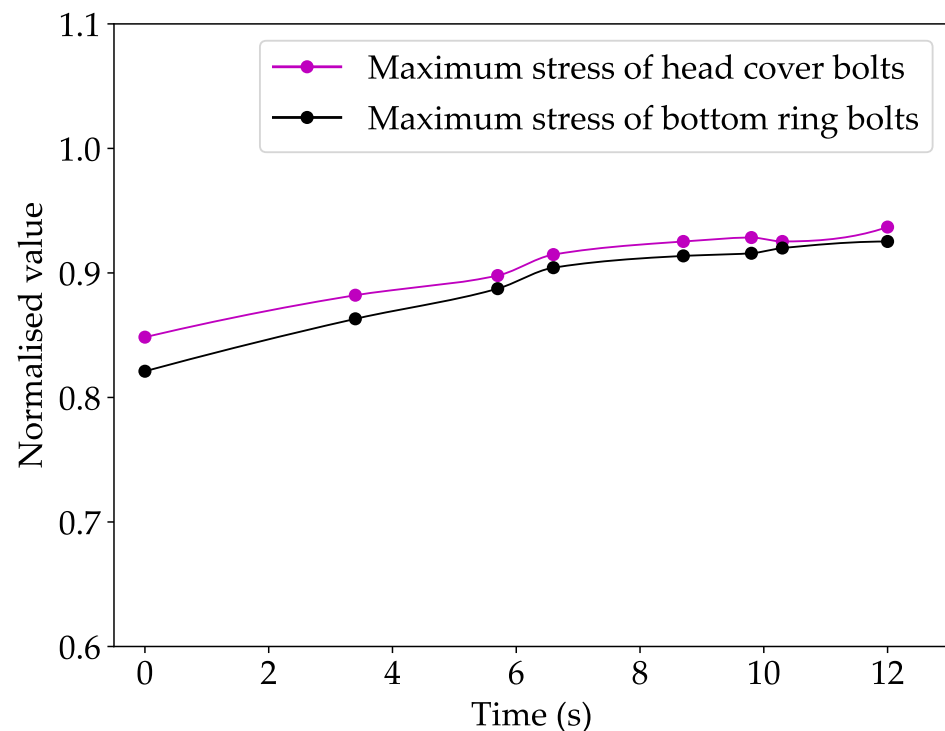


**Figure 13.** The maximum stress of the connecting bolts at different moments during load rejection.

It is strongly recommended that the staff in the power station must strengthen the monitoring of the head cover bolts and bottom ring bolts of the unit, increase the bolt inspection frequency and replace the bolts with a long service time. In the long run, it is recommended to re-optimize the design of the bolt layout of the head cover and bottom ring, preferably using larger nominal diameter bolts.

## 6. Conclusions

This investigation has carried out the characteristic stress analysis of a prototype pump-turbine unit during load rejection based on field measurements and numerical simulation.

The measurement results show that during the transient process of the load rejection, the operating parameters, such as the rotating speed and the pressure at various locations of the flow passages, change drastically.

The measured data are adopted to perform 3D CFD simulations of the unit during load rejection. After the load rejection, the pressures in the spiral case passage and in the draft tube passage are obviously changed due to the effect of the water hammer. The pressure distributions in the crown chamber and band chamber becomes nonuniform. The calculated pressures are used to carry out the flow-induced stresses on the structures and head cover bolts.

The unsteady flow-induced structural stress of the pump-turbine unit during load rejection is changing with time, but the stress distribution at the different moments keeps the same pattern. The maximum stress concentration of the head cover bolts and bottom ring bolts are located at the fillet of the bolt close to the stay ring. The maximum stress of the head cover bolts is higher than the bottom bolts.

The staff in the power station shall strengthen the monitoring of the head cover bolts and bottom ring bolts of the pump-turbine unit and replace the connection bolts with a long service time. It is recommended to use larger nominal diameter bolts to avoid damage to the connecting bolts of the pump-turbine unit.

**Author Contributions:** Conceptualization, Z.W. and X.H.; methodology, X.H.; investigation, X.H., validation, L.C., H.L., S.C., K.H., C.L. and L.Q.; writing—original draft preparation, X.H.; writing—review and editing, X.H., L.C., H.L., S.C., K.H., C.L. and L.Q.; supervision, Z.W. All authors have read and agreed to the published version of the manuscript.

**Funding:** This work was supported by the National Natural Science Foundation of China (No.: 51876099).

**Data Availability Statement:** Not applicable

**Acknowledgments:** The authors would like to express their sincere thanks for the support of the project: Strength analysis and review of bolts for head cover and bottom ring of Yixing pumped-storage power station.

**Conflicts of Interest:** The authors declare no conflict of interest.

### Abbreviations

The following abbreviations are used in this manuscript:

CFD	Computational fluid dynamics
FEM	Finite element method
PSPS	Pumped-storage power station
PT	Pump-turbine
RANS	Reynolds-averaged Navier–Stokes
SST	Shear stress transport

### References

- Liu, X.; Luo, Y.; Wang, Z. A review on fatigue damage mechanism in hydro turbines. *Renew. Sustain. Energy Rev.* **2016**, *54*, 1–14. [[CrossRef](#)]
- Casanova, F.; Mantilla, C. Fatigue failure of the bolts connecting a Francis turbine with the shaft. *Eng. Fail. Anal.* **2018**, *90*, 1–13. [[CrossRef](#)]
- Peltier, R.; Boyko, A.; Popov, S.; Krajisnik, N. Investigating the Sayano-Shushenskaya Hydro Power Plant Disaster. *Power* **2010**, *154*, 48.
- Egusquiza, E.; Valero, C.; Huang, X.; Jou, E.; Guardo, A.; Rodriguez, C. Failure investigation of a large pump-turbine runner. *Eng. Fail. Anal.* **2012**, *23*, 27–34. [[CrossRef](#)]
- Zhao, Q.; Chai, J.; Ma, C.; Ding, J.; Li, B. Causes of Header Bolt Fracture of a Pumped Storage Power Station. *J. Yangtze River Sci. Res. Inst.* **2019**, *36*, 134–138.
- Mandair, S.; Morissette, J.F.; Magnan, R.; Karney, B. MOC-CFD coupled model of load rejection in hydropower station. *IOP Conf. Ser. Earth Environ. Sci.* **2021**, *774*, 12021. [[CrossRef](#)]
- Zhou, D.; Chen, H.; Kan, K.; Yu, A.; Binama, M.; Chen, Y. Experimental study on load rejection process of a model tubular turbine. *IOP Conf. Ser. Earth Environ. Sci.* **2021**, *774*, 12036. [[CrossRef](#)]
- Bi, H.; Chen, F.; Wang, C.; Wang, Z.; Fan, H.; Luo, Y. Analysis of dynamic performance in a pump-turbine during the successive load rejection. *IOP Conf. Ser. Earth Environ. Sci.* **2021**, *774*, 12152. [[CrossRef](#)]
- Zhang, H.; Su, D.; Guo, P.; Zhang, B.; Mao, Z. Stochastic dynamic modeling and simulation of a pump-turbine in load-rejection process. *J. Energy Storage* **2021**, *35*, 102196. [[CrossRef](#)]
- He, L.Y.; Wang, Z.W.; Kurosawa, S.; Nakahara, Y. Resonance investigation of pump-turbine during startup process. *IOP Conf. Ser. Earth Environ. Sci.* **2014**, *22*, 32024. [[CrossRef](#)]
- Kolšek, T.; Duhovnik, J.; Bergant, A. Simulation of unsteady flow and runner rotation during shut-down of an axial water turbine. *J. Hydraul. Res.* **2006**, *44*, 129–137. [[CrossRef](#)]
- Ciocan, G.D.; Iliescu, M.S.; Vu, T.C.; Nennemann, B.; Avellan, F. Experimental Study and Numerical Simulation of the FLINDT Draft Tube Rotating Vortex. *J. Fluids Eng.* **2006**, *129*, 146–158. [[CrossRef](#)]
- Huang, X.; Oram, C.; Sick, M. Static and dynamic stress analyses of the prototype high head Francis runner based on site measurement. *IOP Conf. Ser. Earth Environ. Sci.* **2014**, *22*, 32052. doi:10.1088/1755-1315/22/3/032052. [[CrossRef](#)]
- Goyal, R.; Cervantes, M.J.; Gandhi, B.K. Characteristics of Synchronous and Asynchronous modes of fluctuations in Francis turbine draft tube during load variation. *Int. J. Fluid Mach. Syst.* **2017**, *10*, 164–175. [[CrossRef](#)]

15. Fu, X.; Li, D.; Wang, H.; Zhang, G.; Li, Z.; Wei, X. Dynamic instability of a pump-turbine in load rejection transient process. *Sci. China Technol. Sci.* **2018**, *61*, 1765–1775. [[CrossRef](#)]
16. Avdyushenko, A.; Chernyi, S.; Chirkov, D. Numerical algorithm for modelling three-dimensional flows of an incompressible fluid using moving grids. *Comput. Technol.* **2012**, *17*, 3–25.
17. Widmer, C.; Staubli, T.; Ledergerber, N. Unstable Characteristics and Rotating Stall in Turbine Brake Operation of Pump-Turbines. *J. Fluids Eng.* **2011**, *133*, 41101. [[CrossRef](#)]
18. Nicolle, J.; Giroux, A.M.; Morissette, J.F. CFD configurations for hydraulic turbine startup. *IOP Conf. Ser. Earth Environ. Sci.* **2014**, *22*, 32021. [[CrossRef](#)]
19. Jiang, Y.; Yoshimura, S.; Imai, R.; Katsura, H.; Yoshida, T.; Kato, C. Quantitative evaluation of flow-induced structural vibration and noise in turbomachinery by full-scale weakly coupled simulation. *J. Fluids Struct.* **2007**, *23*, 531–544. [[CrossRef](#)]
20. Egusquiza, E.; Valero, M.; Presas, A.; Huang, X.; Guardo, A.; Seidel, U. Analysis of the dynamic response of pump-turbine impellers. Influence of the rotor. *Mech. Syst. Signal Process.* **2016**, *68–69*, 330–341. [[CrossRef](#)]
21. Huang, X.; Chamberland-Lauzon, J.; Oram, C.; Klopfer, A.; Ruchonnet, N. Fatigue Analyses of the Prototype Francis Runners based on Site Measurements and Simulations. *IOP Conf. Ser. Earth Environ. Sci.* **2014**, *22*, 12014. [[CrossRef](#)]
22. Xie, J.; Huang, B.; Fu, L. Reinforcement and Resonance Control of Head Cover of Francis Turbine by Finite Element Analysis and Modal Testing. *IOP Conf. Ser. Earth Environ. Sci.* **2020**, *560*, 12051. [[CrossRef](#)]
23. Jia, Y.; Li, F.; Wei, X.; Li, X.; Li, Z. A method for analysis of head cover deformation and vibration amplitude in Francis hydro-turbine system by combination of CFD and FEA. *J. Mech. Sci. Technol.* **2017**, *31*, 4255–4266. [[CrossRef](#)]
24. Liang, Q.; Lais, S.; Gentner, C.; Braun, O. Efficient runner safety assessment during early design phase and root cause analysis. In Proceedings of the 26th IAHR Symp. on Hydraulic Machinery and Systems, Beijing, China, 19 August 2012.
25. He, Q.; Huang, X.; Yang, M.; Yang, H.; Bi, H.; Wang, Z. Fluid–Structure Coupling Analysis of the Stationary Structures of a Prototype Pump Turbine during Load Rejection. *Energies* **2022**, *15*, 3764. [[CrossRef](#)]
26. Wang, Z.; Yang, J.; Wang, W.; Qu, J.; Huang, X.; Zhao, W. Research on the Flow-Induced Stress Characteristics of Head-Cover Bolts of a Pump-Turbine during Turbine Start-Up. *Energies* **2022**, *15*, 1832. [[CrossRef](#)]
27. Deng, X.; Li, H.; Huang, S.; Liu, H. Fatigue Life Research on the Connection Bolts of head cover of Pump-Storage Plant. In Proceedings of the 2019 Annual Academic Conference of China Hydropower Engineering Society Power Grid Peak Shaving and Pumped Storage Professional Committee, Beijing, China, 1 September 2019; pp. 156–161.
28. Shahani, A.R.; Shakeri, I. Experimental Evaluation of the Effect of Preload on the Fatigue Life of Bolts. *Int. J. Steel Struct.* **2015**, *15*, 693–701. [[CrossRef](#)]
29. Luo, Y.; Chen, F.; Chen, L.; Wang, Z.; Yu, J.; Zhu, X.; Zhao, Z.; Ren, S.; Li, J.; Lu, X. Study on Stresses of head cover Bolts in a pump-turbine Based on FSI. *IOP Conf. Ser. Earth Environ. Sci.* **2021**, *804*, 42062. [[CrossRef](#)]
30. Luo, Y.; Chen, F.; Chen, L.; Wang, Z.; Yu, J.; Luo, C.; Zhao, Z.; Ren, S.; Li, J.; Deng, D. Stresses and Relative Stiffness of the head cover Bolts in a pump-turbine. *IOP Conf. Ser. Mater. Sci. Eng.* **2019**, *493*, 12113. [[CrossRef](#)]
31. Chen, F.; Chen, L.; Wang, Z.; Yu, J.; Luo, C.; Zhao, Z.; Ren, S.; Li, J.; Deng, D. Computation of Static Stresses of the head cover Bolts in a pump-turbine. *IOP Conf. Ser. Mater. Sci. Eng.* **2019**, *493*, 12143. [[CrossRef](#)]
32. Chen, L.; Li, H.; Yu, J.; Luo, Y.; Wang, Z.; Zhu, X.; Zhao, Z.; Lu, X. Stress Analysis of Screw Connection of Key Structural Components in pump-turbine. *IOP Conf. Ser. Earth Environ. Sci.* **2021**, *804*, 32037. [[CrossRef](#)]
33. Zhao, W.; Huang, X.; Yang, M.; Yang, H.; Bi, H.; He, Q.; Wang, Z. Flow-Induced Dynamic Behavior of Head-Cover Bolts in a Prototype Pump-Turbine during Load Rejection. *Machines* **2022**, *10*, 1130. [[CrossRef](#)]
34. Menter, F.R. Two-equation eddy-viscosity turbulence models for engineering applications. *AIAA* **1994**, *32*, 1598–1605. [[CrossRef](#)]